JOURNAL OF MATERIALS SCIENCE **36** (2001) 4469–4477

Low-cycle fatigue strength under step loading of a Si_3N_4 + SiC nanocomposite at 1350°C

J. DUSZA*
Institute for Advanced Materials, Joint Research Centre, EC, 1755 ZG Petten, The Netherlands

P. ŠAJGALÍK
Institute of Inorganic Chemistry, Slovak Academy of Sciences, Dubravská cesta 9, 842 36 Bratislava, Slovak Republic

M. STEEN
Institute for Advanced Materials, Joint Research Centre, EC, 1755 ZG Petten, The Netherlands

E. SEMERAD
Austrian Research Centers, Seibersdorf, 2444 Seibersdorf, Austria

The low-cycle fatigue behaviour of a hot pressed silicon nitride/silicon carbide nanocomposite and a reference monolithic Si_3N_4 have been investigated in 4-point bending at 1350°C in air using stepwise loading. The nanocomposite was prepared using 20% of SiCN amorphous powder as an additive, together with 5% yttria, to crystalline α-silicon nitride powder. Two types of specimen have been tested, with and without a sharp notch (notch tip radius ~10 μm) at applied loads from 50 N with steps of 25 N and from 50 N with steps of 50 N, respectively. Five cycles have been performed at all applied load levels with an amplitude of 50 N for both types of specimen. The deflection of the specimens has been recorded up to specimen failure. The failure load of the unnotched nanocomposite was significantly higher than that of the monolithic material whereas for the notched specimens only a small difference has been found between the failure loads of the monolithic and the composite. Notched specimens of both materials exhibited a similar size of the slow crack growth area at catastrophic fracture, whereas for unnotched specimens the size of the slow crack growth area was significantly larger for the monolithic ceramic. The nanocomposite exhibits higher fatigue strength due to its higher resistance against stress corrosion damage and stress corrosion crack growth.

1. Introduction

Silicon nitride based materials are one of the most promising candidates for structural application at temperatures around 1350°C. The use of these ceramics as components in gas turbines and advanced automotive engines has received considerable attention over the last years [1]. Systematic research has been carried out with the main goal to optimise the fracture toughness, strength, creep and oxidation resistance [2–5]. The high-temperature properties are mainly controlled by the sintering aids, such as Al_2O_3 + Y_2O_3, Y_2O_3 and Yb_2O_3. Much effort has been made to optimise the type and volume fraction of the additive which is suitable for densification and at the same time exhibits high refractoriness as a grain boundary. Yttria and Ytterbia have been found most refractory at high temperatures and are preferred for applications such as advanced gas turbine engines. Crystallisation of the grain boundary phase by heat treatment after the densification is another possible way to improve its refractoriness [6]. However this method sometimes results in decreasing room temperature fracture toughness and strength. Another method to increase the strength of silicon nitride based ceramics at high temperatures is to disperse crystalline particles (e.g. SiC) with high refractoriness at the grain boundaries [7]. Attention has to be paid, however, not to introduce microcracks into the material caused by the different thermal expansion coefficients of the particles and the matrix. To minimise or avoid microcrack formation, particles with very small size should be used as a dispersoids. During the last years, Si_3N_4 + SiC nanocomposites were developed in which nano-sized SiC particles are dispersed in the Si_3N_4 matrix [8, 9]. These particles are usually located either intragranularly, with a size of approximately 30 nm, or intergranularly with a size of approximately 150 nm [10].

Three main methods have been used for processing such a nanocomposite: hot pressing (HP) or gas

* *Permanent Address*: Institute of Materials Research, SAS, Watsonova 47, 043 53, Kosice, Slovakia.

pressure sintering (GPS) of a mechanical mixture of crystalline Si_3N_4 and SiC powders of sub-micrometer size, HP of a CVD SiCN amorphous powder, and the combination of these methods: HP or GPS of a mixture of a crystalline Si_3N_4 + amorphous SiCN powders [11].

An improvement in mechanical properties compared to monolithic silicon nitride was reported for these composites which is strongly related to the change in microstructure and in chemistry of the composites such as grain morphology, the distribution of SiC particles and the structure and chemistry of grain/phase boundaries and intergranular phases [12–14].

Recent investigations have shown that the microstructure and the high-temperature strength of Si_3N_4 + SiC nanocomposites is strongly influenced by the nucleation step of the nanoparticles before the densification and that the high-temperature strength was improved only when the SiC nanoparticles are located intergranularly [15].

Silicon nitride based ceramics have been intensively tested at high temperatures under different loading regimes and different atmospheres during the last years. Damage regions initiating at the surface of specimens during high temperature tests have been reported by many authors, suggesting that their formation is associated with oxidation [16–18]. During strength and dynamic fatigue testing at high temperatures stress-corrosion cracking was observed as a surface-associated phenomenon consisting of mass removal (cations diffuse to the surface from the bulk and oxygen diffuses inwards) via two-grain and multigrain junctions within the near-surface volume. The phenomena was enhanced under tensile stress [19]. In high temperature fatigue (static and cyclic) the presence of the intergranular glassy phase changes the fatigue mechanisms with respect to room temperature. Since this phase is present to different extents in different materials and since its viscosity is extremely dependent on the chemical composition, the high temperature fatigue behaviour is material dependent. A number of researchers [20, 21] found a "positive fatigue effect" under cyclic loading at high temperatures. This has been attributed to a reduced stress intensity factor at the crack tip caused by loading rate dependent glass phase bridging/blunting of the crack.

During the last five years the high temperature mechanical properties of Si_3N_4 + SiC nanocomposites have been studied by a number of authors [11, 12, 22–25]. It was shown that these ceramics exhibit higher strength and better creep resistance than monolithic Si_3N_4. According to Rendtel *et al*. [22] the strength of Si_3N_4 + SiC nanocomposite at 1400°C lies between 80% and 100% of the room temperature strength with creep rates as low as 1×10^{-9} s^{-1} at 300 MPa and 1400°C. This behaviour can be explained by the thinner and more refractory intergranular phase of the composite compared to the monolithic material. This is caused by trapping of a significant amount of glass between SiC particles and by the presence of carbon in the intergranular phase [23]. Rouxel *et al*. [24] reported rising R–curves in a Si_3N_4 + SiC nanocomposite with a two fold increase in crack growth resistance after 1 mm crack extension. This was explained by time dependent visco-elastic mechanisms which result in rate dependent fracture characteristics. Recently excellent oxidation resistance was reported for Si_3N_4 + SiC nanocomposites compared to monolithic silicon nitride. This was mainly connected with the change in the oxidation and damage mechanisms during operation at high temperatures [25].

There is a lack of high temperature fatigue data on silicon nitride-silicon carbide nanocomposites. Because the large number of specimens necessary for standard fatigue experiments we applied a simple step-wise loading sequence similar to that used in the past by Quinn and Katz for stress-rupture characterisation of silicon nitride [26].

The main purpose of the present contribution is to study the influence of the addition of SiC nano-particles on the deformation and fracture behaviour of silicon nitride under low-cycle fatigue conditions at 1350°C in air.

2. Experimental material and methods

The Si_3N_4 + SiC nanocomposite was prepared using 20% of silicon carbonitride (SiCN) amorphous powder as an additive, together with 5% yttria (grade 4N, Pacific Industrial Development, Ann Arbor, Michigan, USA) to crystalline α-Si_3N_4 powder (grade SN-E10, UBE Industries, Ltd., Japan). The powder mixture was attrition milled in isopropanol for 4 h. The dried starting mixture was sieved through a 25 μm sieve to eliminate large agglomerates. The mixture was cold-pressed in a steel die at a pressure of 100 MPa, then embedded into a boron nitride (BN) powder bed and hot-pressed at 30 MPa and 1750°C under a 2 kPa overpressure of nitrogen. The density of the hot-pressed disks (50 mm diameter) was measured by mercury immersion and exceeded 98% of the theoretical density (TD). The calculated TD was 3.26×10^3 kg/m^3. A reference monolithic ceramic was also prepared to study the influence of SiC particles on crack initiation and propagation during low-cyclic loading at 1350°C. Apart from the addition of amorphous SiCN, all the processing steps, as well as the sintering additive, were the same as for the composite material.

The microstructure of the tested materials was studied by scanning electron microscopy (SEM) on polished and plasma etched samples and by transmission electron microscopy (TEM) and high resolution electron microscopy (HREM) on foils prepared by ion-beam thinning. The size distribution of the inter- and intragranularly located SiC nanoparticles has been evaluated using statistical analysis.

Bend test specimens with a tensile surface finish of 15 μm with dimensions $3 \times 4 \times 45$ mm were cut from the hot pressed discs. The fatigue tests were conducted in four-point flexure (20/40 mm span) at loading/unloading rates of 0.05 mm/min at 1350°C in air.

Two types of specimen have been tested, with and without a sharp notch (notch tip radius $\sim$10 μm) at applied loads from 50 N with steps of 25 N, and from

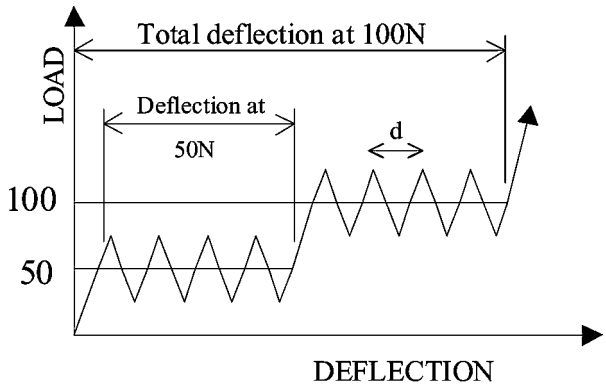

Figure 1 Schematic illustration of the low-cycle fatigue test using step loading of unnotched specimens. The test procedure for notched specimens was the same, but with increasing load steps of 25 N.

50 N with steps of 50 N, respectively. For the specimens with and without a sharp notch $W = 4$ mm and $W = 3$ mm, respectively. Five cycles have been performed at all applied load levels with a loading amplitude of 50 N. The deflection of the specimens has been recorded up to specimen failure and the critical load and deflection at failure were established. Besides this, the deflection after cycling at each load level has been measured too, (Fig. 1).

The failure stress of the unnotched specimens was calculated using the Hollenberg formula [27]:

$$\sigma_{f}' = \sigma_{f}(2n + 1)/(3n) \quad (1)$$

where σ_{f}' is the strength of the crept specimen, n is the flexure creep exponent and σ_{f} is described by:

$$\sigma_{f} = 1.5[P(S_1 - S_2)/BW^2] \quad (2)$$

where P is the failure load, B is the specimen width, W the specimen height, and S_1 and S_2 are the outer and inner span of the four-point bend fixture, respectively. A value of $n = 1.4$ was used for the monolithic as well as the composite material [13].

The applied stress corresponding to slow crack growth initiation in the specimens without a sharp notch has been estimated from the load-deflection curve (deviation from the initial, straight portion of the curve and change in the separation of the cyclic loops, d see Fig. 1 and by using Equation 2. The applied stress intensity factor corresponding to slow crack growth initiation from the notch tip in the specimens with a sharp notch has been estimated in a similar way and calculated using the equation [28]:

$$K_{Ii} = \sigma a^{1/2} Y = \{3F_i(S_1 - S_2)\alpha^{0.5} Y\}/2BW^{1.5}(1-\alpha)^{1.5} \quad (3)$$

with

$$Y = 1.9887 - 1.326\alpha - \{(3.49 - 0.68\alpha + 1.35\alpha^2) \times \alpha(1 - \alpha)\}/(1 + \alpha)^2 \quad (4)$$

where σ is the stress, F_i is the load level at crack initiation, a is the saw notch and depth $\alpha = a/W$ is approximately equal to 0.2. The critical value of the stress intensity factor was also estimated using the above formula under the assumption that linear-elastic behaviour prevails under the testing conditions. In this case $a = a_c$, where a_c is the defect size at fracture (polished notch length + subcritical crack extension), $F = F_f$ is the fracture load and $\sigma = \sigma_f$ is the fracture stress.

According to our previous experiment [29], the nanocomposite contains processing and/or grinding flaws which cause strength degradation and degradation of the dynamic fatigue parameters. To investigate the influence of the SiC addition on the fatigue/creep performance of the Si_3N_4 + SiC nanocomposite specimens where processing/grinding related defects were found as a fracture origin were not taken into consideration for the evaluation.

After mechanical testing the samples were examined using a stereomicroscope at a magnification of $20\times - 100\times$, to determine the notch length and slow crack growth (SCG) size prior to fracture. Fractography was used to study the fracture micromechanisms during slow crack growth.

3. Results and discussion

The microstructure of the nanocomposite consists of Si_3N_4 grains with a bimodal grain-size distribution, (Fig. 2a). Large grains with diameter of ~1.5–2.5 μm with relatively low aspect ratio are observed. The intragranularly located SiC nanoparticles hamper the growth of the Si_3N_4 grains, and locally change their shape, (Fig. 3a). The space between large Si_3N_4 grains is filled by Si_3N_4 and SiC grains ~0.1–0.3 μm in diameter, which results in very small sized (in volume) multigrain junctions. Porosity is present in the microstructure (pores ~0.5 μm in diameter, with occasional coalescence). The relatively homogeneously distributed SiC nanoparticles are located both intergranularly (with a size of approximately 200 nm) or intragranularly (with a size of approximately 50 nm), [13] (See Fig. 4). In agreement with the results of Pan *et al.* [14] HREM revealed the presence of amorphous films on the Si_3N_4/SiC boundaries, but also "clean" boundaries in cases where special crystallographic orientation relationships exists, (Fig. 3b). The monolithic material exhibits a microstructure that is similar to that of the composite; however, with larger average grain diameter and larger multigrain junctions, (Fig. 2b).

Typical load-deflection curves obtained on specimens without sharp notch are illustrated for the nanocomposite (Fig. 5a) and monolithic material (Fig. 5b). The different behaviour is evident. In general, the composite exhibits higher failure load (stress) and therefore withstands higher applied loads and more cycles. Also the composite exhibits less deflection at individual load levels and less total deflection at failure.

In Fig. 6 the total deflection and the accumulated deflection at individual load levels are illustrated for

notched (Fig. 6a) and unnotched specimens (Fig. 6b). For notched specimens the difference in behaviour between the monolithic and the composite is not significant. For monolithic silicon nitride the deflection is slightly higher than for the composite at all applied loads (except at 50 N), and it increases slightly faster with increasing load. This agrees with our previous finding that the fracture toughness of these materials at 1350°C tested at a loading rate of 0.01 mm/min is very similar [10].

For both ceramics the large deflection after cycling at 50 N compared to the deflections at higher load levels is not self-understanding, (Fig. 6a). This phenomenon can be explained by the high stress concentration at the tip of the sharp notch, which allows large deflection due to the high deformation of a small constrained volume of material ahead of the sharp notch. With increasing load, the volume of the deformed material probably increases rapidly, resulting in a lower additional deflection. A second and more possible explanation is that the high stress concentration at the tip of the sharp notch causes crack propagation and therefore relatively high deflection. With increasing load and number of cycles crack-blunting occurs which leads to a decrease of the crack propagation rate and, therefore, a decrease in additional deflection.

The difference in behaviour of the nanocomposite and monolithic silicon nitride is more significant for the unnotched specimens: at all applied load levels the monolithic material exhibits significantly higher "individual" and total deflections than the composite

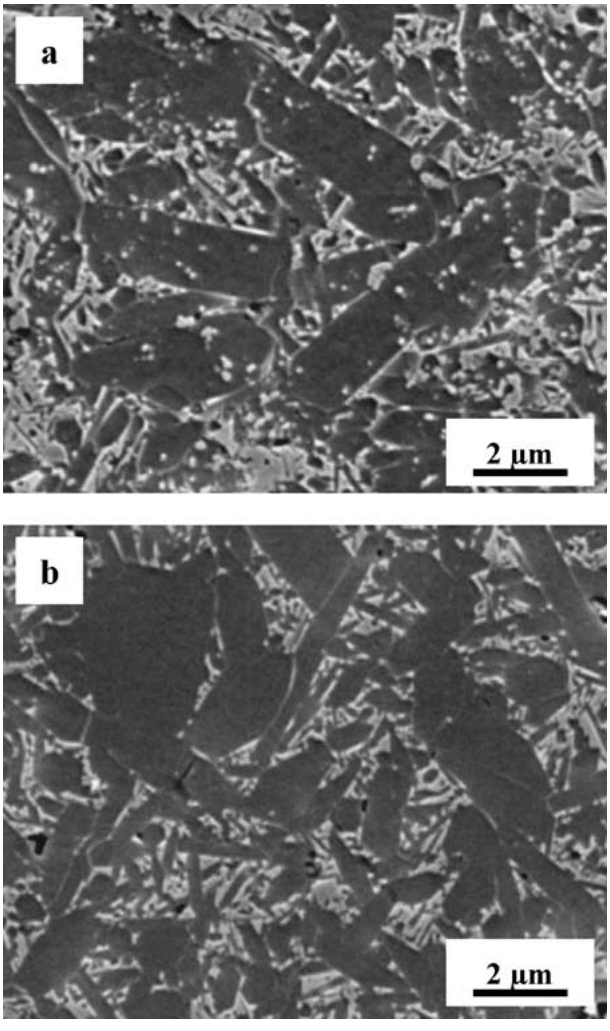

Figure 2 Characteristic microstructure of the investigated materials, (a) Si_3N_4 + SiC nanocomposite, (b) Si_3N_4, (SEM, plasma etched technique).

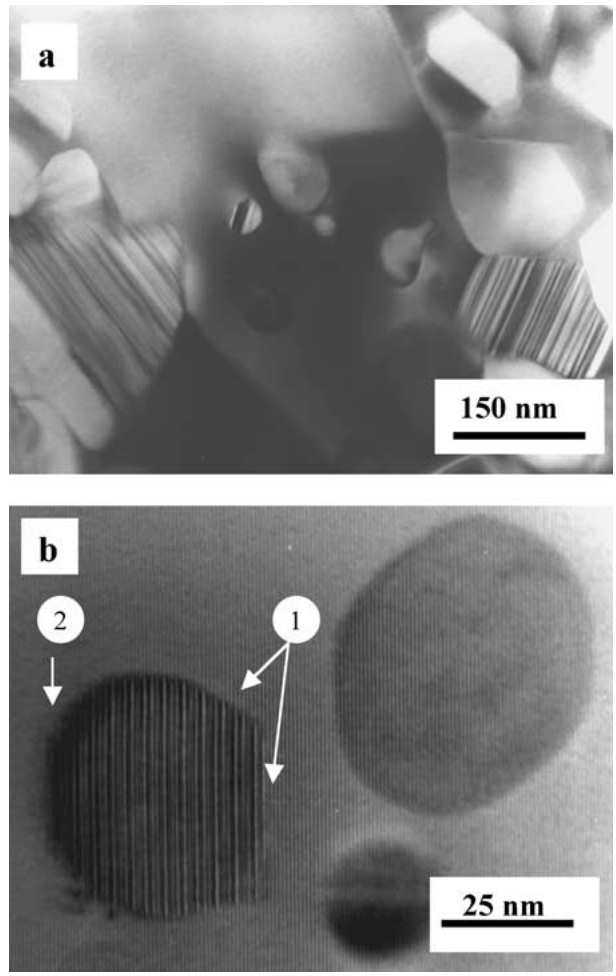

Figure 3 Microstructure of the composite ceramic illustrating (a) pinning of large silicon nitride grains by intergranularly located SiC particles, (b) intragranularly located SiC particles with a clean Si_3N_4/SiC boundary-1 and with an intergranular layer on the boundary-2, (HREM, lattice image technique).

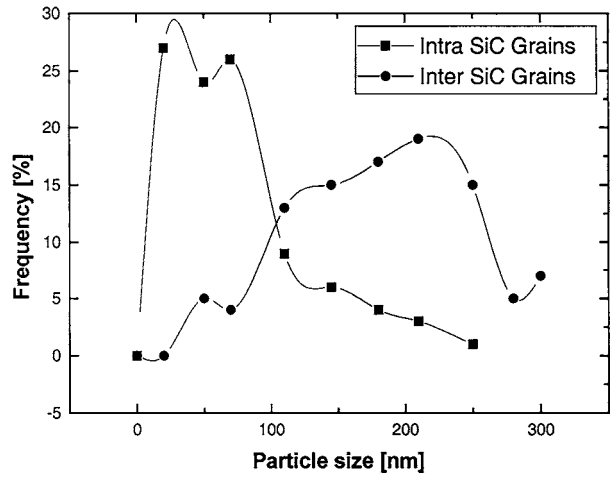

Figure 4 SiC nanoparticle distribution in the composite ceramic.

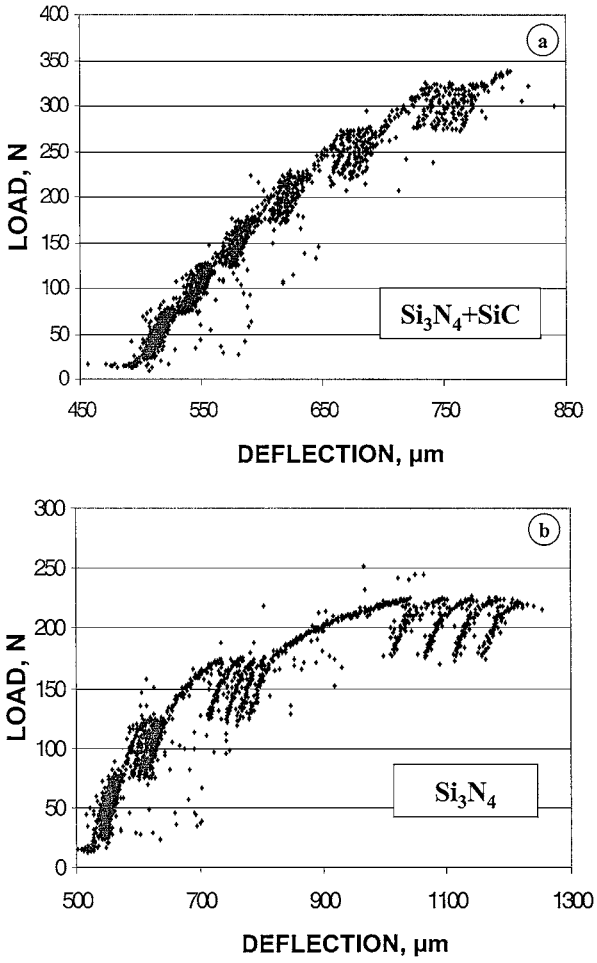

Figure 5 Load-deflection curve for (a) Si_3N_4 + SiC nanocomposite and (b) monolithic silicon nitride.

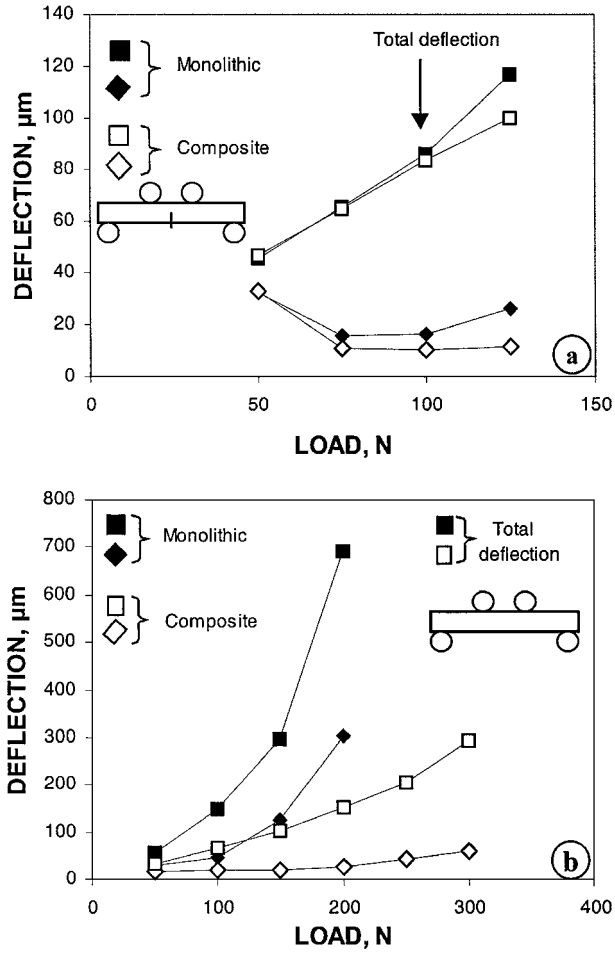

Figure 6 Load-deflection relationships illustrating the deflection of the specimens at individual applied load levels and the corresponding total deflection, (a) notched specimens and (b) unnotched specimens.

(Fig. 6b). This agrees with our previous results which show that the composite exhibits significantly higher creep resistance than the monolithic material in the temperature range from 1200°C to 1400°C [13]. The current results indicate that also in cyclic fatigue/creep conditions the Si_3N_4 + SiC nanocomposite exhibits higher deformation and fracture resistance than monolithic silicon nitride. The significantly different behaviour of monolithic and composite during testing of unnotched specimens shows that the main contribution of the silicon carbide particles probably lies in the deformation and micro-crack initiation process.

SCG prior to catastrophic failure was detected via fractography in both materials and in both, notched and unnotched specimens, (Figs 7 and 8). The shape of the SCG area in notched specimens was usually symmetrical and the crack front was curved, (Fig. 7). The depth of the SCG area at failure was larger near the surface of the samples, which may be related to oxidation-enhanced SCG at the test temperature. The average size of the SCG area in notched specimens (Fig. 7) was very similar for the composite and monolithic ceramic, which corresponds to similar failure loads and fracture toughnesses at 1350°C. The applied stress intensity factor for slow crack initiation in the notched specimens estimated from the load-deflection diagrams and calculated from Equations 3 and 4 is approximately 4.9 $MPam^{0.5}$ for both investigated ceramics. The value of the critical intensity factor in these materials is also very similar, and is equal to 9.1 $MPam^{0.5}$.

On the other hand, the size of the SCG area in unnotched specimens (Fig. 8) was significantly larger in the monolithic material than in the composite. The applied average stress (calculated as an average value of the values for individual specimens) corresponding to slow crack initiation in the unnotched specimens estimated from the load-deflection diagrams and calculated from Equation 2 is 115 MPa for monolithic silicon nitride and 157 MPa for the nanocomposite. The average fracture stress of the monolithic and composite ceramic is 196 MPa and 242 MPa, respectively.

Detailed observation of the SCG area revealed strong oxidation damage located close to the tensile surface of the samples or to the notch tip, (Fig. 9). No significant difference was found comparing the micromechanisms of fracture during SCG in notched and unnotched specimens. On the other hand a significant difference exists between the micromechanisms during SCG in monolithic and composite material, (Fig. 10). The fracture surface of the monolithic Si_3N_4 is more rough compared to that of the composite, and is of mainly intergranular character with a high amount of pull-out

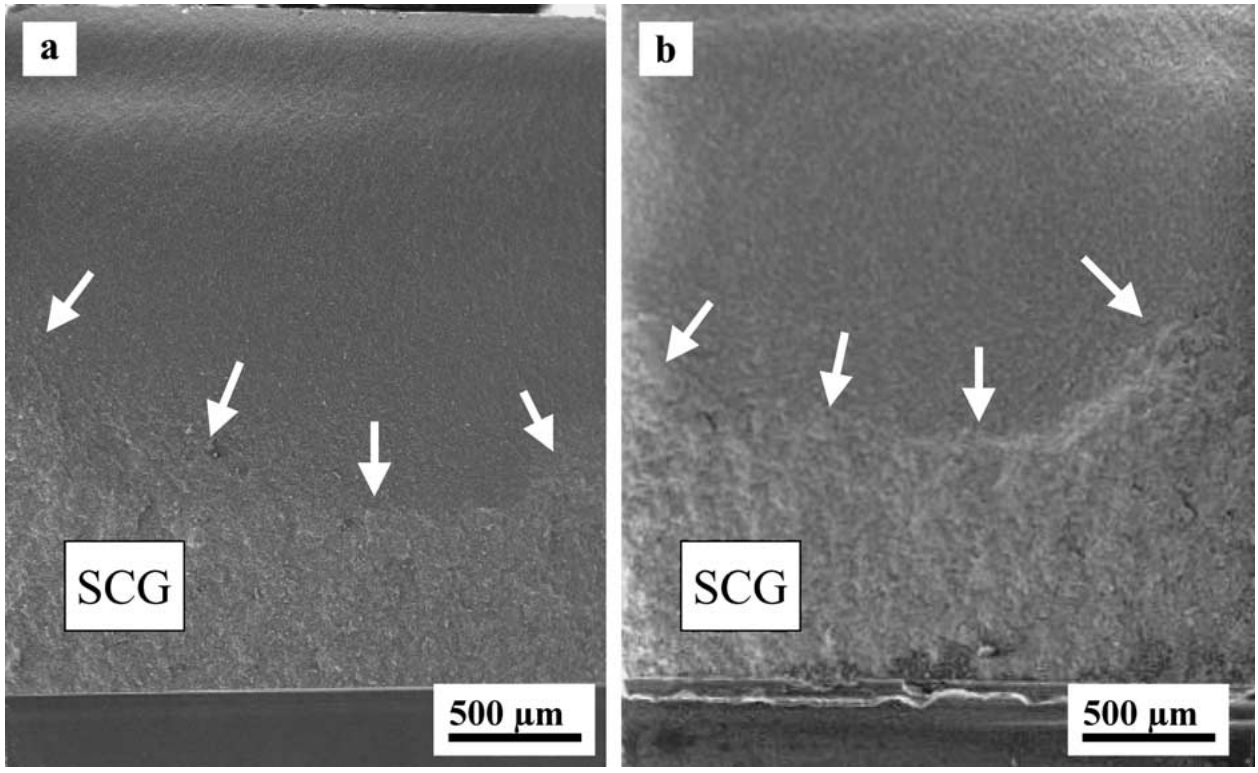

Figure 7 Characteristic fracture surfaces of the notched specimens, (a) Si_3N_4 + SiC, (b) Si_3N_4. Note the curved front of the slow crack growth area which extends deeper near the surface of the specimens due to oxidation assisted crack propagation.

of needle shaped Si_3N_4 grains. For grains that are not orientated perpendicular to the crack plane, this observation means that sliding on Si_3N_4/Si_3N_4 boundaries and deformation of the surrounding microvolume must occur.

The SCG area of the composite was significantly smoother than that of the monolithic Si_3N_4, and the Si_3N_4 grains with larger diameters failed transgranularly. This observation can be explained by the coarser microstructure of the monolithic, and by the hampered sliding and pullout of larger Si_3N_4 grains, via intergranularly located SiC particles in the composite, (Fig. 11). An another possible reason of this phenomenon is that the large Si_3N_4 grains in the nanocomposite are "weaker" due to the intergranularly located SiC nanoparticles which acting as defects and causing the fracture of the grains.

There are two phenomena which determine the low-cycle fatigue strength of the investigated materials: crack initiation and crack propagation. SiC addition may have a double effect. First a change in microstructure (Figs 2 and 11), which seems to have an influence mainly on the crack propagation via the mechanical interaction between the separated fracture surfaces. Secondly a change in volume fraction, in chemical composition and in viscosity of the intergranular phase, which probably affects both crack initiation and propagation [13, 23].

The difference in microstructure between the monolithic and composite material results in different fracture micromechanisms operating during slow crack growth, (Fig. 10). As regards the intergranular phase, our model experiment [13] supports the theory of a decreasing amount of oxide grain boundary phase through the reaction of SiO_2 with carbon, introduced into the microstructure by the addition of SiCN. The presence of SiC particles probably leads to a change in the intergranular phase chemistry and viscosity as well, but our experiments did not confirm this fact, and further investigation is needed to explain this phenomenon.

When testing specimens with a sharp notch the behaviour of the monolithic and composite material is similar. The stress intensity factor corresponding to crack initiation (K_{Ii}) is similar for both materials (4.9 $MPam^{0.5}$), and lies very close to the K_{Ii} value measured for the same materials under constant loading rate (0.01 mm/min), 4.8 and 4.6 $MPam^{0.5}$ for monolithic and composite material [10]. The critical stress intensity factor of 9.1 $MPam^{0.5}$ is similar for both materials, too. Also this agrees with the K_{IC} of 9.5 $MPam^{0.5}$ and 8.0 $MPam^{0.5}$ for monolithic and composite ceramics obtained under constant loading rate. The fracture toughness of a material (PY6, with 6%Y_2O_3) very similar to the monolithic silicon nitride studied here was investigated by Wereszczak *et al.* [30] at high temperatures. The data obtained at 1300°C and 1400°C, approximately 7.0 $MPam^{0.5}$ and 11.6 $MPam^{0.5}$ respectively, are comparable to our results. However as stressed by these authors, too, caution must be exercised in the interpretation because the criteria for application of linear-elastic fracture mechanics may be not truly valid for the considered testing conditions.

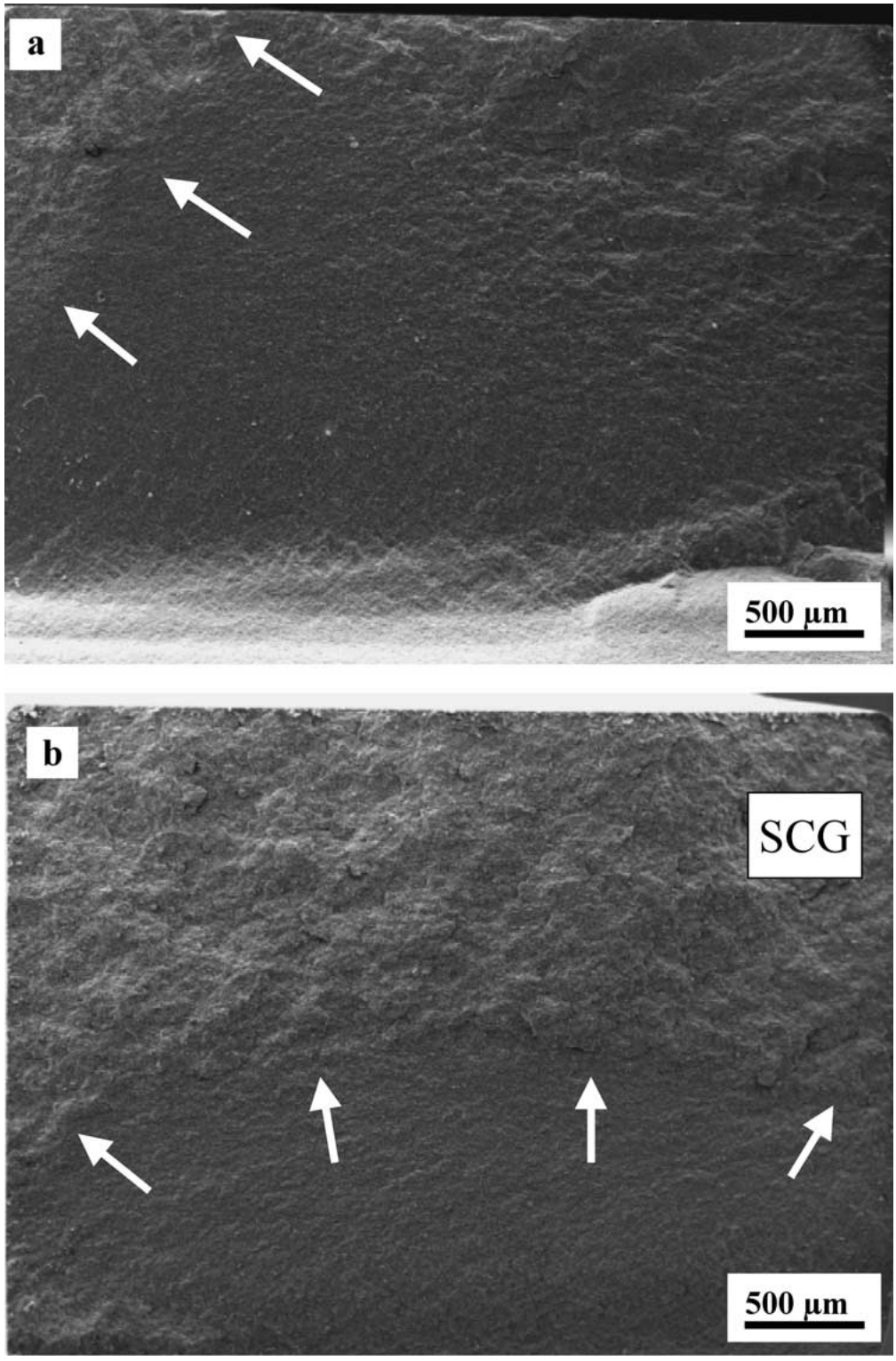

Figure 8 Characteristic fracture surfaces of the unnotched specimens, (a) Si_3N_4 + SiC nanocomposite (b) Si_3N_4. Note the different size and shape of the slow crack growth area in the monolithic and composite ceramics.

It seems that the most important factor controlling the fatigue strength of the investigated materials is crack initiation and the initial stage of crack growth, both of them probably strong related to the oxidation phenomena. For the monolithic material the observations of Wereszczak *et al*. [17, 19] are confirmed, and oxygen transport into the grain boundaries and cation diffusion to the surface probably alters the microstructure and leads to weakening of the mechanical integrity of the grain boundaries. Because this process is stress enhanced, it can be significant even during the relatively short period which the specimens spent at 1350°C under a rising load. Our observations indicate that a number of microcracks originate simultaneously from the tensile surface of the specimen, but only one among these propagates relatively fast under stress corrosion cracking caused by stress concentration and accumulation of

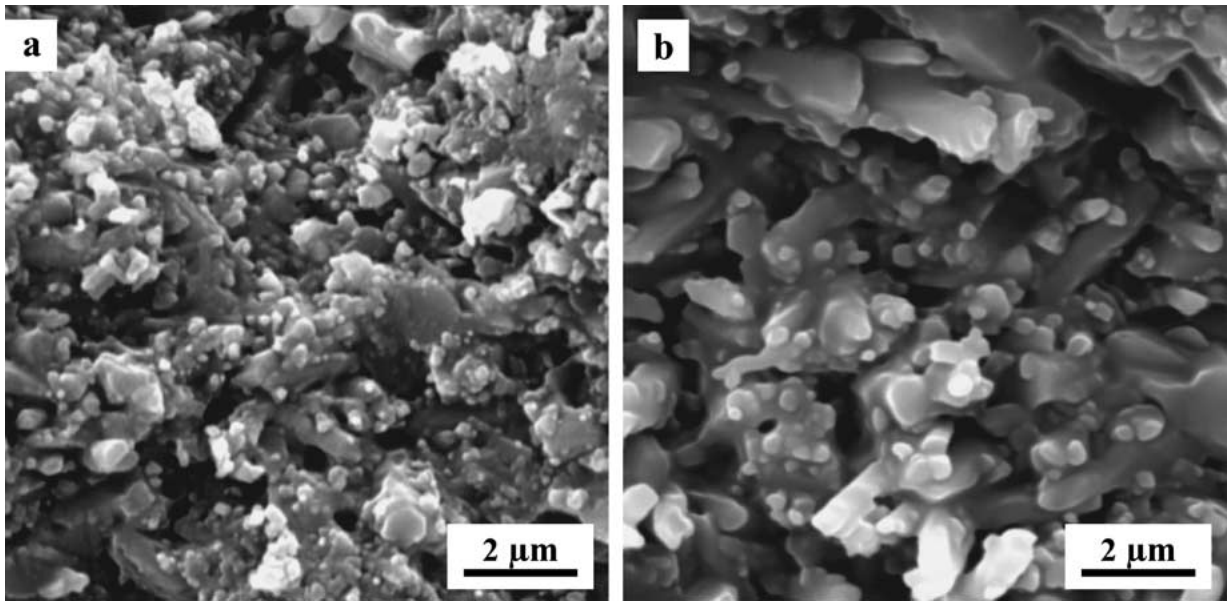

Figure 9 Details of the slow crack zone/stress corrosion cracking zone close to the tensile surface of the specimens with clearly visible oxidation damage, (a) Si_3N_4 + SiC composite, (b) Si_3N_4.

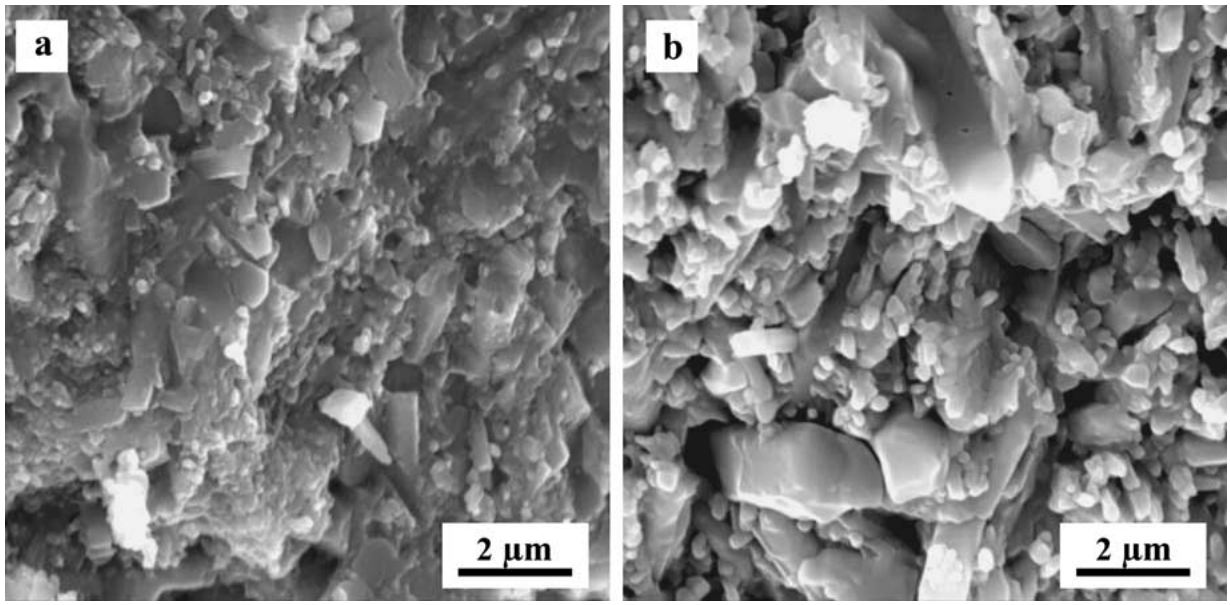

Figure 10 Details of the slow crack zone/stress corrosion cracking zone far from the tensile surface of the specimens (a) Si_3N_4 + SiC composite, (b) Si_3N_4. The different fracture micromechanisms during slow crack growth in both materials are clearly visible.

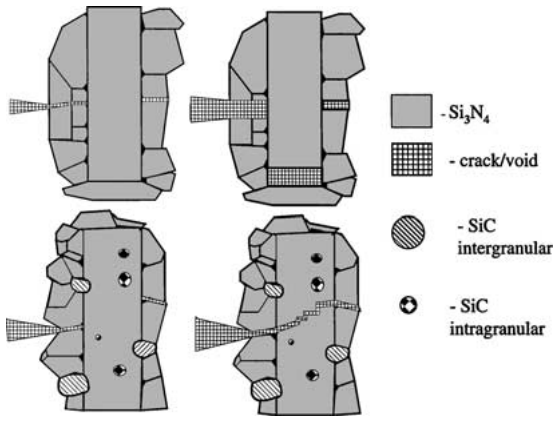

Figure 11 Schematic illustration of the differences in crack propagation in silicon nitride (top) and composite (below). Note pinning of silicon nitride grains by intergranular SiC particles, which prevents their pulling out during crack propagation.

oxygen and metal cation impurities in the vicinity of its tip.

The situation in the Si_3N_4 + SiC nanocomposite is different due to the intergranularly located SiC particles which result in a smaller individual multigrain junctions and probably in a thinner intergranular phase (or even its absence) on the Si_3N_4/SiC boundaries. This, together with the lower volume fraction and probably change in chemical composition of the intergranular phase results in a limited oxygen transport through the grain boundaries into the volume of the material, (Fig. 12). Probably, this is the main reason that the formation and growth of corrosion cracks in the composite material is slower than in the monolithic ceramic, resulting in a higher fatigue strength of the composite.

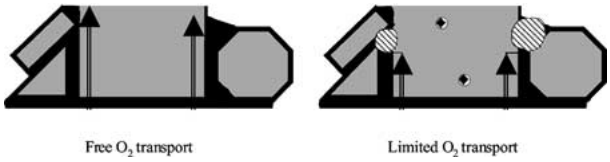

Figure 12 Schematic illustration of differences in oxidation transport into the bulk of the material in silicon nitride (left) and composite (right). Note the presence of intergranular SiC particles which lower the volume fraction of the intergranular phase, reduce the size of the multigrain junctions and probably change the chemical composition of the intergranular phase.

4. Conclusions

A silicon nitride-silicon carbide nanocomposite was fabricated from a powder mixture of amorphous SiCN and crystalline α-Si_3N_4 powder with 5 wt% of Y_2O_3 additive. The influence of the addition of SiC nanoparticles on the low-cycle fatigue behaviour under step loading has been investigated at 1350°C in air by comparing the data obtained on the nanocomposite and on the monolithic silicon nitride fabricated using the same processing steps as the composite. The nanocomposite exhibits higher fatigue strength than the monolithic material. This is caused by the higher resistance against the initiation and propagation of corrosion cracks as a result of the intergranularly located SiC particles which decrease the effective "cross section" of the intergranular phase and limit the oxygen transport into the bulk of the material.

Acknowledgement

The work was carried out during J. Dusza's stay at the Institute for Advanced Materials, Joint Research Centre, Commission of the European Communities in Petten, The Netherlands and at Austrian Research Centers Seibersdorf in Seibersdorf, Austria. The work was partially supported by the Slovak Grant Agency under the contract number VEGA 2/1166/21. The authors express their thanks Dr. P. Hvizdos for TEM investigation of the studied materials.

References

1. M. MATSUI, *Ceram. Int.* **19** (1993) 9.
2. P. F. BECHER, E. Y. SUN, K. P. PLUCKNETT, K. B. ALEXANDER, CH-H. HSUEH, H.-T. LIN, S. B. WATERS, C. G. WESTMORELAND, E. S. KANG, K. HIRAO and M. E. BRITO, *J. Amer. Ceram. Soc.* **81** (1998) 2821.
3. E. Y. SUN, P. F. BECHER, K. P. PLUCKMETT, CH-H. HSUEH, K. B. ALEXANDER, S. B. WATERS, K. HIRAO and M. E. BRITO, *ibid.* **81** (1998) 2831.
4. H. INAMURA, K. HIRAO, M. E. BRITO, M. TORIJAMA and S. KANZAKI, *ibid.* **83** (2000) 495.
5. R. RAJ, *ibid.* **76** (1993) 2147.
6. M. K. CINIBULK, G. THOMAS and S. M. JOHNSON, *ibid.* **81** (1990) 1606.
7. F. F. LANGE, *ibid.* **56** (1973) 445.
8. K. NIIHARA, K. SUGANUMA, A. NAKAHIRA and K. IKAZI, *J. Mater. Sci. Lett.* **9** (1990) 598.
9. K. NIIHARA, K. IZAKI and T. KAWAKAMI, *ibid.* **10** (1990) 112.
10. J. DUSZA, P. ŠAJGALÍK and M. STEEN, *J. Amer. Ceram. Soc.* **82** (1999) 3113.
11. J. DUSZA and M. STEEN, *Int. Mat. Rev.* **44** (1999) 165.
12. M. HERRMANN, C. SCHUBERT, A. RENDTEL and H. HÜBNER, *J. Amer. Ceram. Soc.* **81** (1998) 1095.
13. P. ŠAJGALÍK, M. HNATKO, F. LOFAJ, P. HVIZDOF, J. DUSZA, P. WARBICHER, F. HOFER, R. RIEDEL, E. LECOMTE and K. RAJAN, *J. Europ. Ceram. Soc.* **20** (2000) 453.
14. X. PAN, J. MAYER and M. RÜHLE, *J. Amer. Ceram. Soc.* **79** (1996) 389.
15. H. PARK, H.-E. KIM and K. NIIHARA, *J. Europ. Ceram. Soc.* **18** (1998) 907.
16. Y. G. GOGOTSI and G. GRATHWOHL, *J. Amer. Ceram. Soc.* **76** (1993) 3093.
17. A. A. WERESZCZAK, T.P. KIRKLAND, K. BREDER, M. K. FERBER and P. KHANDELWAL, *Mat. Sci. Eng.* **A191** (1995) 257.
18. T. OHJI, Y. YAMAUCHI, W. KANEMATSU and S. ITO, *J. Mater. Sci.* **25** (1990) 2990.
19. A. A. WERESZCZAK, M. K. FERBER, T. P. KIRKLAND, K. L. MORE, M. R. FOLEY and R. L. YECKLEY, *J. Amer. Ceram. Soc.* **78** (1995) 2129.
20. D. BOLSCH and J. BRESSERS, in Proc. 1st European Ceramic Society Conf., Maastricht, The Netherlands, 1990, edited by G. de With *et al*., Vol. 3, pp. 205–209.
21. S. Y. LIU, I. W. CHEN and T. Y. TIEN, *J. Amer. Ceram. Soc.* **77** (1994) 137.
22. A. RENDTEL, H. HÜBNER, M. HERRMANN and C. SCHUBERT, *ibid.* **81** (1998) 1109.
23. J.-L. BESSON, M. MAYNE, D. BAHLOUL-HOURLIER and P. GOURSAT, *J. Europ. Ceram. Soc.* **18** (1998) 1893.
24. T. ROUXEL, F. WAKAI and S. SAKAGUCHI, *J. Amer. Ceram. Soc.* **77** (1994) 3237.
25. M. HERRRMANN, H. KLEMM, B. GÖBEL, C. SCHUBERT and W. HERMEL, *Key Eng. Mat.* **161–163** (1999) 377.
26. G. QUINN and R. N. KATZ, *Ceram. Bulletin* **57** (1978) 1057.
27. G. W. HOLLEMBERG, G. R. TERWILLIGER and R. S. GORDON, *J. Amer. Ceram. Soc.* **54** (1971) 196.
28. J. KÜBLER, *Ceram. Eng. Sci. Proc.* **18** (1997) 155.
29. J. DUSZA, P. ŠAJGALÍK, M. STEEN and E. SEMERAD, *Mat. Sci. Eng.* **A291** (2000) 250.
30. A. A. WERESZCZAK, M. K. FERBER, R. R. SANDERS, M.G. JENKINS and P. KHANDELWAL, *Ceram. Eng. Sci. Proc.* **14** (1993) 101.

Received 22 June 2000
and accepted 7 May 2001